Journal of Hydrology 630 (2024) 130669

Contents lists available at ScienceDirect

Journal of Hydrology

journal homepage: www.elsevier.com/locate/jhydrol

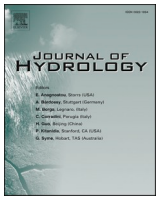

Research papers

Delving into flash droughts in Vietnam during the last two decades using the standardized evaporative stress ratio

Ngoc My Nguyen [a,b], Minha Choi [c,d,*]

[a] School of Civil, Architectural, and Environmental System Engineering, Sungkyunkwan University, Suwon 440-746, Republic of Korea
[b] Department of Global Smart City, Sungkyunkwan University, Suwon 440-746, Republic of Korea
[c] School of Civil, Architectural Engineering and Landscape Architecture, Sungkyunkwan University, Suwon 440-746, Republic of Korea
[d] Department of Water Resources, Graduate School of Water Resources, Sungkyunkwan University, Suwon, 440-746, Republic of Korea

ARTICLE INFO

This manuscript was handled by Dr marco borga, Editor-in-Chief, with the assistance of Dhais Peña-Angulo, Associate Editor

Keywords:
Vietnam
Flash drought
Standardized Evaporative Stress Ratio
ENSO

ABSTRACT

A flash drought is a recently defined extreme event that has destructive impacts on agriculture as well as other elements of society and ecosystems. Understanding where and when flash droughts occur can improve predictability and mitigation strategies for countries with economies that rely on agriculture. This study represents the first investigation of flash drought occurrences in Vietnam, one of the largest agricultural exporters in the world, using the standardized evaporative stress ratio (SESR). Monthly SESR data captured historical sustained drought events across the study period and exhibited a pattern similar to that shown by the standardized precipitation evapotranspiration index over most of the study region, with Pearson's correlations mostly ranging from 0.52 to 0.82. Results of the SESR analysis at a pentad timescale indicate that flash droughts did occur in the country over the last two decades, with the northern regions and a majority of the south-central coast experiencing fewer than 9 flash drought events that covered less than 20% of each region. The remaining southern areas of the country were subjected to a much higher flash drought frequency, with 12 to 21 occurrences covering from 30% to more than 50% of the area in each region, typically during the dry season and exacerbated by anomalies of potential evapotranspiration and temperature. This research also revealed that flash droughts in Vietnam were correlated with the El Niño Southern Oscillation climate phenomenon, particularly in the southern regions, where a high flash drought frequency could take place under either El Niño or neutral conditions. This study provides new evidence to support the development of a comprehensive overview of drought in Vietnam, the country's drought mitigation strategies, and water management policies.

1. Introduction

Droughts are among the most damaging natural hazards and an extreme phenomenon worldwide (Smith and Katz, 2013) due to their detrimental effects on water supplies, ecosystems, agricultural production, and society (Narasimhan and Srinivasan, 2005; Godfray et al., 2010; Hu et al., 2019). Physically, a conventional drought event manifests as a prolonged deficit in water storage and flux that can disrupt longstanding hydrological balances (Hobbins et al., 2016). Notwithstanding the gradual and long-lasting features of traditional droughts, a kind of drought event characterized by rapid intensification has been identified: a flash drought (Hobbins et al., 2016; Wang et al., 2016; Forda and Labosier, 2017). Initially, a flash drought occurs as a meteorological drought that can rapidly switch to an agricultural drought when climatic conditions deteriorate; it is sometime termed an agricultural flash drought (Christian et al., 2019). The speedy onset and evolution of drought is caused by severe atmospheric anomalies, including the absence of rainfall, strong winds, high surface temperatures, and clear skies, that last for several weeks. This combination of anomalies results in rapid land-surface desiccation via excessive evaporative demand from the atmosphere regardless of prior moisture conditions (Christian et al., 2019), significantly shortening the time available to mitigate the impacts of drought (Otkin et al., 2015). A flash drought commonly has large effects on crop yields, can result in economic losses (Hu et al., 2019; Li et al., 2020), and is likely to cause greater agricultural and social devastation than evolving sustained

* Corresponding author at: School of Civil, Architectural Engineering & Landscape Architecture, Sungkyunkwan University, 2066 Seobu-ro, Suwon 16419, Republic of Korea.
E-mail address: mhchoi@skku.edu (M. Choi).

https://doi.org/10.1016/j.jhydrol.2024.130669
Received 7 June 2023; Received in revised form 30 October 2023; Accepted 26 December 2023
Available online 23 January 2024

droughts (Otkin et al., 2015). As such, a better understanding of where and when flash droughts are likely to occur is needed to improve the ability to predict them and implement mitigation strategies, particularly in countries with economies dominated by agriculture.

As one of the world's largest agricultural exporters, Vietnam has a long history of cultivation, one that has played a fundamental role in the rapid development of its economy (Paul et al., 2004). Vietnam frequently suffers substantial economic losses due to droughts, which are ranked third among costly natural hazards (Nguyen and Shaw, 2011). Quantifying drought is therefore of paramount importance to the country. The nation's mainland is wholly located in a tropical climate that is likely to experience severe droughts, particularly during El Niño Southern Oscillation (ENSO) events (Lyon, 2004), and has high potential for flash drought occurrence (Christian et al., 2021). Besides, along with the global warming, the mean air temperature has been speedily increasing across Vietnam at a rate of 0.26 ± 0.10 °C per decade since 1971, which is approximately twice the global rate for the same period (Nguyen et al., 2014).

Despite widespread recognition of this threat, few studies (Zaki and Noda, 2022) have examined the changes, probability, and frequency of droughts in Vietnam (Thanh et al., 2014; Tue et al., 2015; Le et al., 2020, 2019). Those studies have improved understanding of drought in Vietnam, but shortcomings and ambiguities in the research need to be clarified. For example, most of these studies analyzed the evolution of meteorological droughts using a drought index based only on precipitation (P) (i.e., the standardized precipitation index) (Thanh et al., 2014; Tue et al., 2015), which can fail to capture the effects of warming on drought severity (Vicente-Serrano, 2010). Thanh et al. (2014) applied drought indices based on a combination of P and air temperature, such as Peday's and Martonne index. This work reflected the effect of global warming on Vietnamese droughts, but these used drought indexes that may underestimate the severity of extreme drought events because of a lack of information on the interactions between soil moisture and evapotranspiration (Aghakouchak et al., 2014). Specifically, an indicator that incorporates evapotranspiration, which plays a central role in energy-water exchange between land surfaces and the atmosphere, would better track drought characteristics (Yao et al., 2010; Kim and Rhee, 2016). Based on that understanding, Le et al. (2019) and Le et al. (2020) applied the multivariate Palmer drought severity index and standardized precipitation evapotranspiration index (SPEI), respectively, to assess drought conditions in Vietnam. Those two indexes incorporate potential evapotranspiration (PET), as estimated by the Thornthwaite equation, to reflect the involvement of warming in drought severity (Vicente-Serrano et al., 2010). However, a major debate about global drought trends has arisen due to the difference between PET calculated by the Thornthwaite equation and those calculated by the Penman-Monteith equations (Dai, 2012). Zhou et al. (2020) also pointed out that a temperature-based method (i.e., the Thornthwaite equation) significantly underestimates PET, compared with the output of other popular radiation-based (i.e., Priestley and Taylor) and energy balance-based (Penmann–Monteith) methods, implying that drought indices that rely on Thornthwaite-derived PET do not adequately capture the characteristics of drought extremes.

Previous studies concentrated on prolonged drought events, leaving a critical scientific question unanswered: What are the characteristics of Vietnam flash droughts? With the extreme devastation that flash droughts can cause to agricultural operations in mind, it is critical to understand where and when flash drought events occur over the country. This research thus attempts to answer that question and improve the country's capacity to predict flash droughts and to develop mitigation strategies. Given that a drought can be viewed as 'flash' event when moisture-stress conditions intensify rapidly (Otkin et al., 2018), a novel percentile-based methodology proposed by Christian et al. (2019) relied on standardized evaporative stress ratio (SESR) was used in this research due to its ability to comprehensively assess all the flash drought criteria. In general, the main objective of this study is to pinpoint the characteristics of flash drought in Vietnam by analyzing SESR-based drought index. This study attempts to answer two main scientific questions:

(1) What are the characteristics of flash drought events in Vietnam?
(2) What is the relationship between ENSO and flash droughts in Vietnam?

2. Study area

Vietnam is a southeast Asian country on the Indochinese Peninsula, between 101.1 °E and 110.3 °E and 8.2 °N and 23.5 °N. Topographically, one-quarter of the country's territory is covered by plains interspersed with hills and mountains. The remaining three-quarters are mountains and hills that form an arc stretching from the northwest to the southeast of the country and facing the East Sea. The north, south, and southwest of mainland are adjacent to the East Sea. Vietnam has 3,260 km of coastline and thousands of islands and archipelagos. The entire country has a tropical climate; the northern half has a tropical monsoon climate with 4 distinct seasons, and the southern half is a tropical monsoon with 2 seasons. For example, northern Vietnam has a relatively cold winter, whereas the south experiences a warmer winter. While the north experiences scorching temperatures in the summer, the south enjoys cooler conditions. With a hot and humid climate, Vietnam has cultivated a prosperous agriculture industry by devoting more than 70 % of its land area to farming, making the country one of the top rice producers in the world with many other agricultural products such as rice paddy, coffee, soybeans, and corns.

Due to the complex topography and climatology of Vietnam, this study divided the country into seven sub-regions: the North Mountains and Midlands (R1), Red River Delta (R2), North Central Coast (R3), South Central Coast (R4), Central Highlands (R5), Southeast (R6), and Mekong River Delta (R7), as shown in Fig. 1 and Table 1. Being under the influence of monsoons and topography, two sub-regions, R1 and R2, have four distinct seasons yearly, consisting of a dry and cold winter (from December to February), a tepid spring (from March to May), a sweltering and humid summer (from June to August), and a mild autumn (from September to December). Sub-region R3 has four seasons similar to those of the two northern sub-regions, but experiences warmer temperatures during winter. All four southern sub-regions have two seasons, including a dry season (from the end of November to April) and a rainy season (from May to November). Coastal sub-regions R4 and R7 are hot year-round, whereas both R5 and R6 experience cooler weather (Fig. 1). Overall, three sub-regions in the north experience large variations among the seasons, with wide amplitudes of air temperature, while four sub-regions in the south experience regularly hot weather with less fluctuation in air temperature (Fig. 1). Using those differences in climatic conditions among regions, we established the study at either regional or national mainland scales to investigate spatial–temporal changes in flash drought events from 2003 to 2021.

3. Materials

3.1. Global land evaporation amsterdam model (GLEAM)

The GLEAM is a satellite-based global evapotranspiration dataset, providing adequate information of actual evapotranspiration (AET), PET, and several other hydrological variables, such as the components of land evapotranspiration and surface and root-zone soil moisture (Miralles et al., 2011). This product was generated to maximize consolidation of satellite observations and provide spatial–temporal continuity of terrestrial evapotranspiration at a resolution of 0.25° on a daily scale. The model applies the Priestley and Taylor equation to compute daily PET using surface available energy and air temperature, and then downscale PET to AET using a dimensionless coefficient parameterizing the resistance to evapotranspiration. The method might accurately

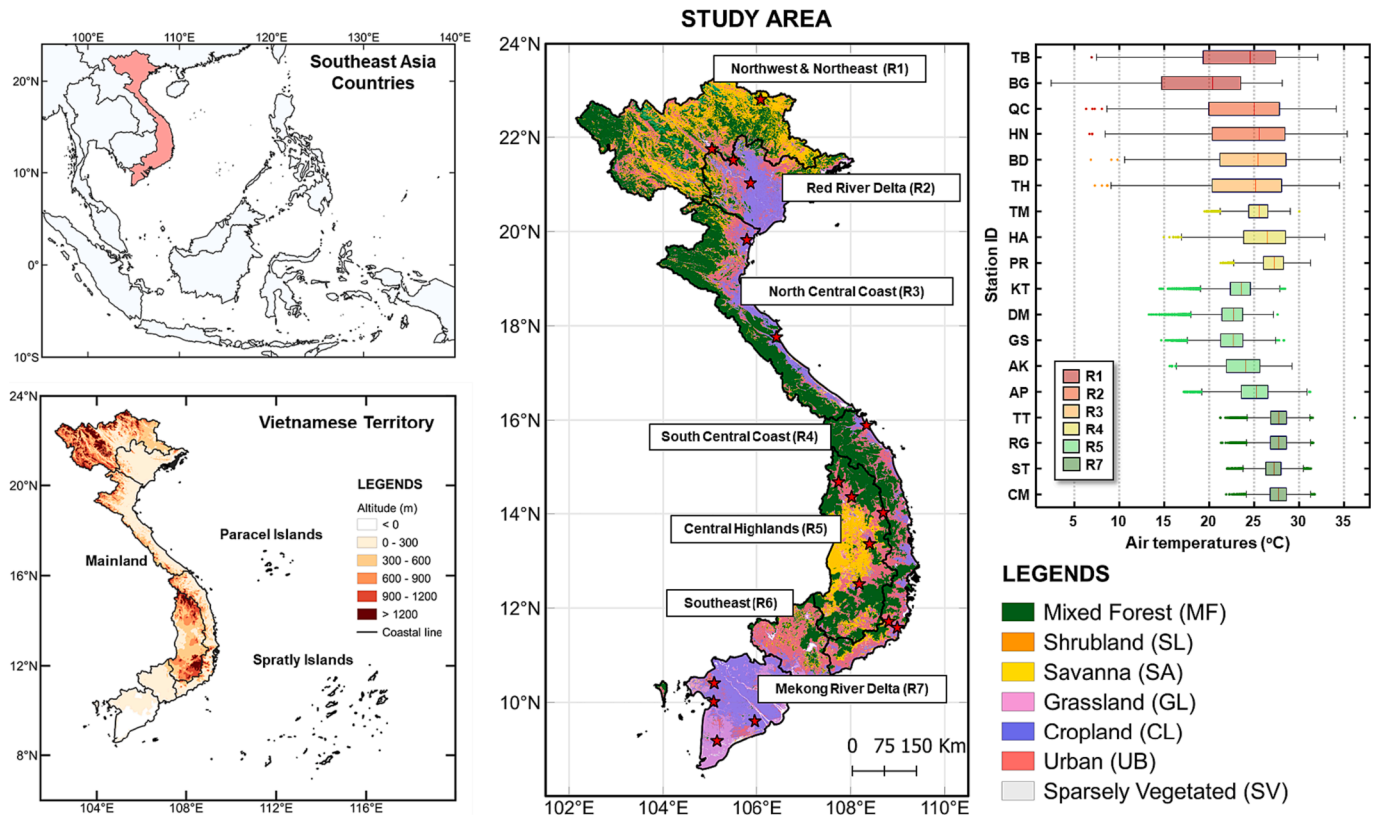

Fig. 1. Land cover classification of the study region, geographic locations, altitudes, and annual variations in air temperature over the 18 ground stations used in the study.

Table 1
Dominant land cover and dominant climate types for each sub-region of Vietnam.

Sub-region	ID	Dominated land cover	Dominated climate type (ID)*
Northwest & Northeast	R1	Grasslands & Mixed Forests	Temperate, dry winter, hot summer (Cwa)
Red River Delta	R2	Croplands	Temperate, dry winter, hot summer (Cwa)
North Central Coast	R3	Cropland & Mixed Forests	Tropical, monsoon (Am)
South Central Coast	R4	Cropland & Mixed Forests	Tropical, savannah (Aw)
Central Highlands	R5	Cropland & Mixed Forests	Tropical, savannah (Aw)
Southeast	R6	Croplands	Tropical, monsoon (Am)
Mekong River Delta	R7	Croplands	Tropical, savannah (Aw)

*This information summarized in the Table is referred from Beck et al. (2018).

calculate AET when compared with the well-known Penmann-Monteith and Priestley-Taylor Jet Propulsion Laboratory approaches (Miralles et al., 2016). In this study, the latest version 3.6b of GLEAM, which is based solely on satellite data from January 1, 2003, to December 31, 2021, was downloaded to retrieve AET and PET data. Then, GLEAM dataset covering mainland of Vietnam (7.8911 °N to 23.3933 °N and 101.6250 °E to 110.1250 °E) was subset for using in this study.

3.2. Integrated Multi-satellite Retrievals for global precipitation measurement

Global Precipitation Measurement (GPM) is a partnership between the US National Aeronautics and Space Administration and the Japan Aerospace Exploration Agency that provides global precipitation data at a high temporal and spatial resolution. The GPM level 3 product uses the Integrated Multi-satellite Retrievals for GPM (IMERG) system, which incorporates all available precipitation data from ground-gauge analyses, microwave-calibrated infrared data, satellite-microwave precipitation data, and other sources with half-hourly temporal and 0.1° × 0.1° spatial resolutions (Huffman, 2018). The IMERG system generates three types of products: Early, Late, and Final runs, which have response times of 4 h, 12 h, and approximately 2 months, respectively, after observation (Huffman et al., 2020). The Early and Late run types are conducted in near real-time and adjusted with climatological coefficients that change by location and month. The Final run type is produced post-real-time when gauge calibration is consistent with precipitation data supplied by the Global Precipitation Climatology Centre. The Final run product is more accurate than other versions, particularly over land, and is the most appropriate dataset for scientific research.

We used the Final run product of the latest IMERG (GPM_3IMERGDF_V06) to retrieve P data for the study period. P for the mainland of Vietnam (7.8911 ^{o}N to 23.3933 ^{o}N and 101.6250 ^{o}E to 110.1250 ^{o}E) was the first subset, which was then upscaled to the pixel size of the GLEAM data for further calculations. The temporal length of the P dataset was 3 months shorter than the GLEAM dataset due to the time limit of IMERG products.

3.3. Climate indices

To examine the influence of ocean processes on drought events in Vietnam, popular climatic indexes incorporating El Niño and La Niña events were used. The Oceanic Niño Index (ONI), as defined by NOAA Climate Prediction Center, is a primary indicator that monitors seasonal climate patterns over the ocean domain, namely ENSO. The ONI index tracks higher- and lower-than-normal sea-surface temperatures in the east-central tropical Pacific Ocean using running 3-month means. The Southern Oscillation Index (SOI) is one measurement of large-scale air-

pressure fluctuations, including El Niño and La Niña events, over the region between the western and eastern tropical Pacific Ocean (Kiladis and van Loon, 1998). The SOI is standardized from observations of sea-level pressure to distinguish between the island nation of Tahiti and Darwin, Australia. Nino3.4 is a widely used index to define El Niño and La Niña episodes based on the average equatorial sea-surface temperature over a region stretching from the international dateline to the South American coast (Trenberth and Stepaniak, 2001). The multivariate ENSO index (MEI) is a temporal record of a leading combined empirical orthogonal function incorporating five key climatic variables (i.e., outgoing longwave radiation, sea-level pressure, sea-surface temperature, and the zonal and meridional components of surface winds) across the tropical Pacific basin (Wolter and Timlin, 1993; 1998). The *trans*-Niño index (TNI) quantifies the gradient in anomalies of sea-surface temperature between the central and eastern equatorial Pacific Ocean, which is measured as (Niño1 + 2) – (Niño4) (Trenberth and Stepaniak, 2001). These five climate indices were used to examine the association between ENSO modes and flash drought events in Vietnam. They can be download from https://psl.noaa.gov/data/climateindices/list, and include the study period (2003–2021).

4. Methodology

4.1. Standardized evaporative stress ratio drought index

4.1.1. Calculations

The SESR index was first proposed by Christian et al. (2019) to identify flash droughts by accounting for their fundamental drought features of a short duration and a large effect. SESR calculations contain AET and PET, both of which are highly sensitive to rapid changes in soil moisture and evaporative stress (ET_{stress}) in the atmosphere, and reflect the effects of radiation, humidity, temperature, and wind anomalies, all of which are involved in the intensification of flash droughts (Otkin et al., 2013). The SESR was computed using data from GLEAM, which provides an adequate and reliable dataset of daily AET, its components, PET, and soil moisture (Miralles et al., 2011). The SESR quantifies flash drought events using the concept of evaporative stress ratio (ESR) using AET and PET:

$$ESR = \frac{AET}{PET} \tag{1}$$

where ESR varies within the range [0,1]. ESR values close to 0 indicate that moisture in the soil and vegetation meets little or none of the evaporative demand from the atmosphere. Values approaching 1 indicate that the available moisture on the land surface satisfies a majority or all of the evaporative demand from the atmosphere. Generally, the larger the ESR the lower the stress of evapotranspiration in the environment, and vice versa.

To avoid volatility in detecting flash drought events, the daily ESR were converted to a pentad scale (5-day mean) (Christian et al., 2019). Next, a standardized ESR was calculated from the pentad ESR to support comparisons of ET_{stress} among different regions and of ESR values over long time periods. The pentad ESR values were computed for each pixel as follows:

$$SESR_{ijk} = \frac{ESR_{ijk} - \overline{ESR_{ijk}}}{\sigma_{ESR_{ijk}}} \tag{2}$$

where $SESR_{ijk}$ is the *z*-score of ESR for a specific pixel (*i,j*) at the time of pentad *k* and $\overline{ESR_{ijk}}$ and $\sigma_{ESR_{ijk}}$ are the mean and standard deviation, respectively, of ESR at a specific pixel (*i,j*) and the time of pentad *k* for all available years during the study period.

To identify the 'flash' characteristic of drought, the pentad-to-pentad change of SESR ($\Delta SESR$) was calculated at each pixel over the study duration. These changes were standardized in the same manner:

$$\left(\Delta SESR_{ijk}\right)_z = \frac{\Delta SESR_{ijk} - \overline{\Delta SESR_{ijk}}}{\sigma_{\Delta SESR_{ijk}}} \tag{3}$$

where $\left(\Delta SESR_{ijk}\right)_z$ is the z-score of the change in the SESR for a specific pixel (*i,j*) at the time of pentad *k*, and $\overline{\Delta SESR_{ijk}}$ and $\sigma_{\Delta SESR_{ijk}}$ are the mean and standard deviation of the SESR changes, respectively, at a specific pixel (*i,j*) and the time of pentad *k* for all available years during the study period.

4.1.2. Flash drought detection

To define whether a drought qualifies as 'flash' event, four criteria were thoroughly evaluated based on the SESR and ΔSESR at each pixel, following Christian et al. (2019):

(1) The declining SESR must last for at least six pentads, equivalent to five ΔSESR.
(2) The final SESR value of the duration should fall below the 20th percentile of the SESR.
(3) The third criterion includes two components: (3a) ΔSESR should be equal to or less than the inter-pentad 40th percentile value; and (3b) only one ΔSESR is allowed to be larger than 40th percentile value following a ΔSESR that satisfies criterion 3a. When criterion 3b is met, the following ΔSESR must reach criterion 3a and have a final ΔSESR of a flash drought event smaller than the SESR value of the two previous pentads.
(4) The mean value of ΔSESR over the entire flash drought duration must be under the threshold of the 25th percentile value of the climatological changes in SESR at that pixel and time of year.

The percentile thresholds used in criteria 2 and 3 were retrieved from the data variability of SESR and ΔSESR for each local pixel and specific pentad of all years during study period. The percentile thresholds applied in criteria 4 were computed using the ΔSESR for all pentads of a flash drought event at a local pixel level.

4.2. Standardized precipitation evapotranspiration index (SPEI)

To evaluate the SESR performance, PET data from GLEAM products were utilized not only to compute the SESR but also to replace the Thornthwaite-based PET in the SPEI calculations in current work. Because PET in GLEAM products was retrieved using observations of near-surface air temperature and surface net radiation based on the Priestley and Taylor algorithms (Miralles et al., 2011), which efficiently calculate PET values similar to those generated by the Penmann–Monteith method (Zhou et al., 2020). The SPEI was selected for comparison because it is simpler than the Palmer drought severity index (Vicente-Serrano, 2010), and superior to the Standardized Precipitation Index in taking warming into account when quantifying drought severity (Beguería et al., 2014).

By definition, the SPEI is based on the climatic water balance, known as the difference between P and PET. We computed the SPEI following a procedure described by Vicente-Serrano (2010) with two main steps:

(1) The accumulation of water deficit D_W (D_W = P − PET) was calculated at 1-month timescales for each pixel to better examine seasonal drought variations.
(2) To obtain the SPEI, D_W was normalized into a log-logistic probability distribution using two equations:

$$F_{(\chi)} = \left[1 + \left(\frac{\alpha}{\chi - \gamma}\right)^{\beta}\right]^{-1} \tag{4}$$

$$SPEI = W - \frac{c_0 + c_1 W + c_2 W^2}{1 + d_1 W + d_2 W^2 + d_3 W^3} \tag{5}$$

where $F_{(\chi)}$ is the probability distribution function of variable D_W, and α, γ, and β are the respective scale, origin parameters, and shape of the log-logistic distribution (Vicente-Serrano, 2010; Yao et al., 2018). With $P(D_W) \leq 0.5$, $W = \sqrt{-2\ln(P(D_W))}$, where $P(D_W) = 1 - F(\chi)$; with $P(D_W) \geq 0.5$, $(1 - P(D_W))$ is used instead of $P(D_W)$ and the sign of the SPEI is reversed.

4.3. Other examining methods

4.3.1. Statistical analyses

The modified Mann–Kendall (MMK) trend test (Hamed and Rao, 1998) and Sen's slope (Sen, 1968) were used to examine trends in precipitation, ET_{stress} (which measures differences between PET and AET), and flash drought conditions in the study regions. The MMK test, which statistically evaluates the monotonic trends of hydrological variables over time, was selected because it is a widely used non-parametric test with low requirements for data distribution and quality. The robustness of the MMK test allows it to consider the effects of autocorrelated time series that can affect trend results (Hamed and Rao, 1998). Sen's slope, which is also a well-known non-parametric method, was chosen because it is not sensitive to outliers and is regularly applied to assess trends in univariate meteorological and hydrological time series (Hamed, 2009; Gocic and Trajkovic, 2013). We conducted an inter-comparison of the SESR and SPEI and an examination of the linkage between those drought indexes and ENSO phases at each grid point within the study region using Pearson's correlation (R). Values of R range within [−1,1], with a larger R representing a higher correlation between these two indices and vice versa (Nguyen and Choi, 2022).

4.3.2. Features of drought dynamics

Temporal and spatial patterns of flash drought were examined using frequency of occurrence (f_D) and drought area percentages (PDA), respectively (Le et al., 2020). f_D and PDA are calculated using the following equations:

$$f_D = \frac{\sum_{j=1}^{n} Du_j}{N} \times 100\% \quad (6)$$

where Du_j is the j^{th} flash drought duration detected using frameworks described in Section 4.1.2; n is the total number flash drought duration at a specific pixel, and N is the number of pentads during study periods, and

$$PDA_{(m)} = \frac{A_{DA}}{A_{Total}} \times 100\% \quad (7)$$

where A_{DA} is the number of pixels with flash drought conditions and A_{Total} is the total number of pixels within the regions.

5. Results and discussion

5.1. Characteristic of climate over seven sub-regions

5.1.1. Annual variation of P and ET_{stress}

To the best of our knowledge, no previous studies have focused on ET_{stress} in the atmosphere in Vietnam despite the fact that the climate features across southeast Asia are strongly affected by the annual change in surface-atmosphere circulation (Le et al., 2019). This section examines annual variability not only in P but also in ET_{stress}, estimated as the difference between PET and AET (PET − AET), as shown in Fig. 2.

The annual patterns of both P and ET_{stress} differ between the northern and southern regions. The northern regions (R1–3) generally have relatively high P magnitudes (nearly 200 to 500 mm month^{-1}) from May (the end of spring) to October (the middle of the fall), whereas the rainy months in the southern regions (R4–7) last longer, from May to November, but with lower amounts (nearly 200 to 400 mm month^{-1})

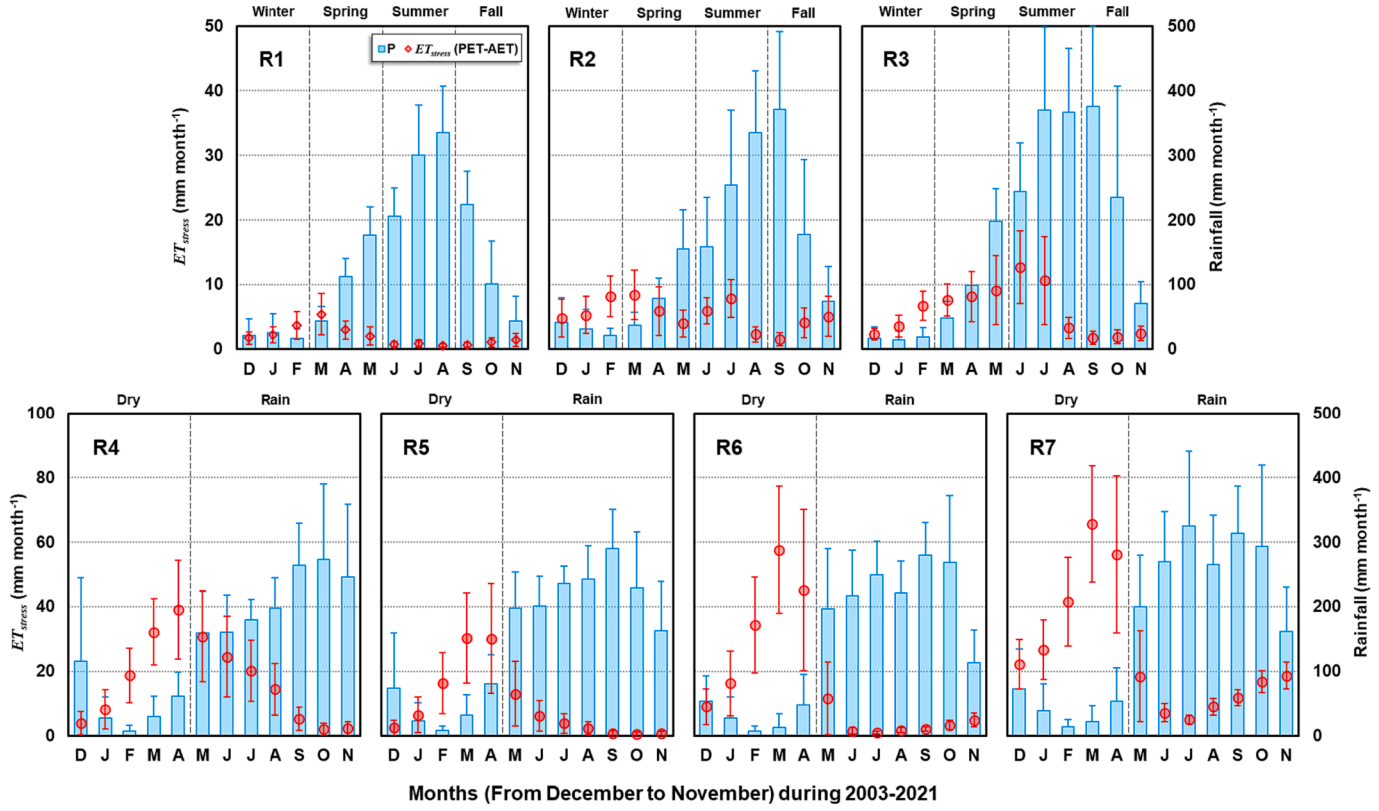

Fig. 2. Annual cycles of precipitation (P) and evaporative stress (ET_{stress}, difference between potential and actual evapotranspiration) across seven sub-regions of Vietnam. Blue and red vertical lines illustrate ± standard deviation of P and ET_{stress}, respectively.

during peak time. The dry period of regions R1–3 lasts from November (the end of fall) to April (the middle of spring) with little P (from 20 to 80 mm month^{-1}), during winter, when P is below 40 mm month^{-1}. The dry season in regions R4–7 (December to April) showed slightly higher P (mostly above 40 to more than 100 mm month^{-1}) compared with (R1–3) during same period. ET_{stress} is small in regions R1–3 (mostly below 10 mm month^{-1}) and increases toward regions R4–R7 (reaching nearly 70 mm month^{-1} in R7), with distinct patterns in annual change. Region R1 showed lower ET_{stress} compared with R2 and R3, where small ET_{stress} values were common during winter and spring, and an insignificant ET_{stress} (close to 0) was seen during summer and fall. ET_{stress} in region R2 randomly fluctuated during the one-year course, but remained relatively large, at nearly 10 mm month^{-1} during winter (January to March), with a low P or during summer (June and July), with a large P amount. In R3, ET_{stress} had a similar increasing tendency with P, which started in winter and reached a peak of approximately 12 mm month^{-1} in the hot summer (June and July), but ET_{stress} then steadily declined during the peak of the rainy months (August and September). All four southern regions (R4–7) had much higher ET_{stress} during the dry season, in which the south-central region (R4 and R5) has approximately 40 mm month^{-1} of ET_{stress} and the southeast regions (R6 and R7) approached 70 mm month^{-1} of ET_{stress} at peak time. After peak time, ET_{stress} in R4 gradually decreased when the rainy season began and hit bottom in October, while ET_{stress} in R5–7 rapidly declined immediately after the onset of the rainy season. A significant intensification of ET_{stress} was observed in R7, beginning in July, under rainy weather. Overall, the northern regions (R1–3) annually have much wetter conditions than do the southern regions (R4–R7). While moisture deficit in R1–3 may occur either in the cold (and dry) season (R1 and R2) or in the hot (and rainy) season (R2 and R3), the southern R4 and R5 regions mostly experienced an extreme surface dryness during the dry season. One feature in common between the R3 and R4 central coast regions is that, during hot conditions, the moisture deficit is not robustly sensitive to P, with steady increases (R3) and decreases (R4) expected with rainfall escalations.

Compared with regions R4–7, regions R1–3 experienced a larger amplitude of air temperature (Fig. 1) that varied seasonally in a pattern that matched that of P (Le et al., 2019). Lower air temperatures during the winter may generate a small evaporative demand in the atmosphere (Donohue et al., 2010) regardless of low P conditions, and high P may supply water for extreme evaporative demand caused by scorching hot temperatures during summer. However, ET_{stress} may still occur during the sultry summer despite relative rainy conditions in R2 and R3, and in R3 in particular, revealing the potential for droughts to occur in these regions under such weather. In southern regions R4–7, the massive ET_{stress} during the dry season was due primarily to its significantly low P and constantly high air temperature, particularly in R7, which had the highest mean temperature (Fig. 1) in the country. In addition, the increasing trend in ET_{stress} magnitude from the northern R1 region toward the southern R7 region was similar to trends in mean temperature across the stations in the seven sub-regions (Fig. 1), suggesting a dependence of ET_{stress} on air temperature rather than on P in study region. Among the regions, R1 commonly experienced lower air temperatures than R2 and R3, which can be attributed to the effects of the high elevations of this region (Fig. 1) (Le et al., 2019); ET_{stress} in R1 was correspondingly lower than in R2 and R3. Although it was within the rainy months, ET_{stress} in R3–4 still showed a steady change due to steep terrain and narrow hills, which have minimal water-holding capacity, resulting in a moisture deficit in the regions. Overall, these findings indicate that ET_{stress} was much higher in the southern R4–7 regions than in the northern R1–3 regions, particularly during the dry months. ET_{stress} conditions in Vietnam are generally not strongly disturbed by P due to the hot weather and complex typography of the country, which potentially leads to differences in drought quantification between P-based and ET-based indexes.

5.1.2. Inter-annual variation of P and ET_{stress}

To further examine the long-term trends in P and ET_{stress}, results of MMK tests, illustrated as spatial maps in Fig. 3 and Fig. 4, were used to describe inter-annual and inter-seasonal tendencies and slopes, respectively, during the study period.

At an inter-annual time scale, MMK analysis revealed that P had increased in R1 and R2 and mostly decreased in R3–7 (Fig. 3). Along with the increase in annual P in the northern R1 and R2 regions, a significant decline of ET_{stress} was observed in the same regions at such time scales. However, despite a decrease of P in R3–7, ET_{stress} also tended to decrease in large portions of these regions, except the Central Highlands (R5) and small areas of R3 and R4 and R7, where ET_{stress} increased. At inter-seasonal time scales, P in the northern R1 and R2 regions mostly increased during winter and fall and decreased during spring. While P in region R3 primarily declined from winter to summer and only increased slightly in the fall over a majority of the region, P in regions R4–7 likewise increased only during wintertime (early periods of dry season) and tended to decrease during rest of the year. R1 was associated with a significant decrease in ET_{stress} from fall to spring and an insignificant decrease during summer, whereas R2 showed a significant decline throughout the year. ET_{stress} in R3–7 showed a decrease over the majority of the area year-round, except for a central portion of R4 and a western portion of R5, where ET_{stress} was likely to increase during the late dry and early rainy seasons (a seasonal change period). The Mekong River Delta in R7 and southeast region R6 experienced an increase in ET_{stress} during the spring and summer, respectively. Overall, P in northern R1–3 regions primarily increased during winter and fall and decreased during spring, and P in southern R4–7 regions tended to increase during the early months of the dry season and primarily decreased in the rest of year. ET_{stress} showed a notable decrease in the northern R1 and R2 regions as well as a majority of other regions year-round, except for a central portion of R4 and a western area in R5 with an increase during seasonal change period.

As can be seen in Fig. 4, the inter-annual increase rate for P was highest in R1 and R2 (>10 mm year^{-1}), which was consistent with a report by Le et al. (2020). The inter-seasonal investigation in this study revealed that the highest increase rate of these regions only occurs during fall seasons, and these regions even experienced a slight decrease in P (<5 mm season^{-1}) during spring. In other R3-7, the inter-annual decrease amounts of P were the largest (>20 mm year^{-1}) in the South Central Coastal (R4), Highland (R5) and Mekong River Delta (R5), which was in close agreement with Le et al. (2020). However, P in these regions increased (>5 mm season^{-1}) during winter and decreased during the rest of the one-year course. When it comes to ET_{stress}, a large decrease (>2 mm year^{-1}) over time was seen over a majority of the country. The northern R2 region experienced a large decline in magnitude at the inter-annual (>2mm year^{-1}) and inter-seasonal (>1.5 mm season^{-1}) timescales, which can be attributed to the effect of an increase in P during the same period (Figs. 3 and 4) as well as a reduction in air temperatures (Le et al., 2020). Likewise, the inter-annual growth (>2 mm year^{-1}) of ET_{stress} was the highest in the Central Highlands (R5), which experienced the highest escalation of air temperatures in the country (Le et al., 2020). Our inter-seasonal comparison found that this large increase in ET_{stress} primarily occurred during the late dry and early rainy seasons. Again, these results indicate that ET_{stress} in Vietnam is sensitive to air temperature, particularly during rapid increases in temperatures over the southern regions (Le et al., 2020). These results also support the essential value of using ET-based rather than P-based indicators to quantify drought in Vietnam.

5.2. Performances of SESR in Vietnam

As the SESR is the key variable in the drought analysis used in this study, this section thoroughly evaluates the performance of monthly SESR based on the SPEI in quantifying drought conditions over the region of interest. *R* (a correlation coefficient) was used to make inter-

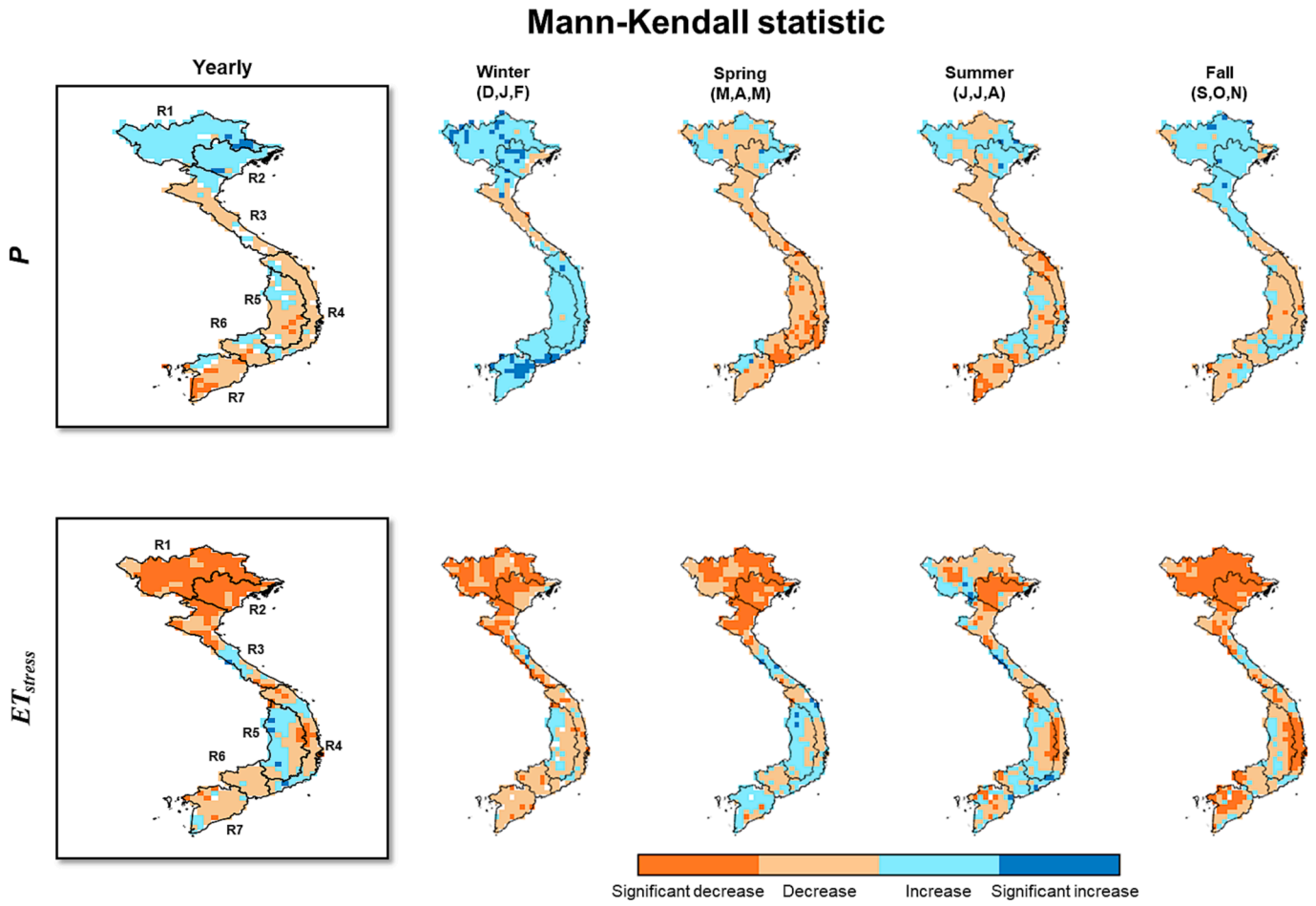

Fig. 3. Mann-Kendall trend test of yearly and seasonal precipitation (P) and evaporative stress (ET_{stress} = PET-AET) during the study period (2003–2021) in Vietnam.

comparisons of these two indexes via a spatial map and boxplots (Fig. 5). Also, monthly time series between these two drought indexes were constructed over seven sub-regions (Fig. 6) to describe their temporal variations during study period.

Correlations between the SESR and SPEI clearly varied among sub-regions. These two indices were most closely correlated in the south-east (R6) and Mekong River Delta (R7), with mean *R* values reaching 0.79 and 0.82, respectively (Fig. 5). Lower but consistent correlations were observed in the north (R1 and R2) and Central Highlands (R5), with average *R* values of approximately 0.58, 0.52, and 0.59, respectively. While the weakest correlation between these two indices was found in sub-regions R3 and R4, with a mean value for *R* of approximately 0.22 and 0.41, respectively, and *R* frequently dropping below 0 (Fig. 5b), particularly in R3. However, the SESR and SPEI generally followed a similar pattern in temporal variations during study periods, which also agrees closely with the historical record (pink shades in Fig. 6) of Vietnam droughts. For example, both the SESR and SPEI effectively captured the historical drought events in R4 and R5 in 2003 (Stojanovic et al., 2017), in R7 in 2019–2020 (Ty et al., 2022) and over the entire country in 2004–2005, 2010, and 2014–2016 (Stojanovic et al., 2017; Le et al., 2020; Ty et al., 2022). However, the SPEI frequently showed less extreme drought severity than did the SESR, including the drought events taking place in 2004–2005 across the country. In regions R3 and R4, the SPEI also regularly predicted the beginning and ending of drought events sooner than those predicted by the SESR. Overall, the SESR efficiently captured historical drought events during study periods, proving its usefulness in depicting drought conditions in Vietnam. Also, the SESR was strongly and positively correlated with SPEI over a majority of regions, except R3 and R4, where the two indexes mainly presented negative correlations and inconsistences in quantifying drought characteristics.

By definitions, the SPEI and SESR track drought events that rely on a deficit between P and PET (Beguería et al.,2014) and the ratio between AET and PET (Christian et al., 2019), respectively. A drought event detected by the SPEI technically begins and ends at the same time with a shortage P period, while droughts quantified by SESR have starting and ending phases identical to those of periods with high ET_{stress}. Incorporating the results described in Section 5.1.1, it is clear that regions R5–7 regularly experience large ET_{stress} during the dry season, with extremely low P (Fig. 2). Likewise, regions R1 and R2 annually experience a small amount of ET_{stress}, in which greater ET_{stress} primarily takes place during the dry winter and spring. The two indices capture a similar period of drought and correlate closely with each other over these regions. By contrast, ET_{stress} in R3 remains low during the dry winter but higher during spring and summer, with increasing P magnitudes (Fig. 2). Drought events captured by the SPEI in such regions therefore tend to start from a dry winter while those by the SESR are likely to begin later, when ET_{stress} begins to intensify. Similarly, ET_{stress} in R4 inherently remains high during the dry season and changes insignificantly when the rainy season begins (Fig. 2); drought events captured by the SPEI in this region potentially end when P begins escalating while those captured by the SESR last longer.

Not surprisingly, the SPEI is more accurate than the other P-based drought indices (i.e., Palmer drought index and Standardized Precipitation index) (Beguería et al., 2014), but it is less efficient than the evapotranspiration-based drought index in monitoring agricultural drought due to a lack of AET in its computations (Beguería et al., 2014; Pei et al., 2018). Including PET in SPEI calculations only reflects the

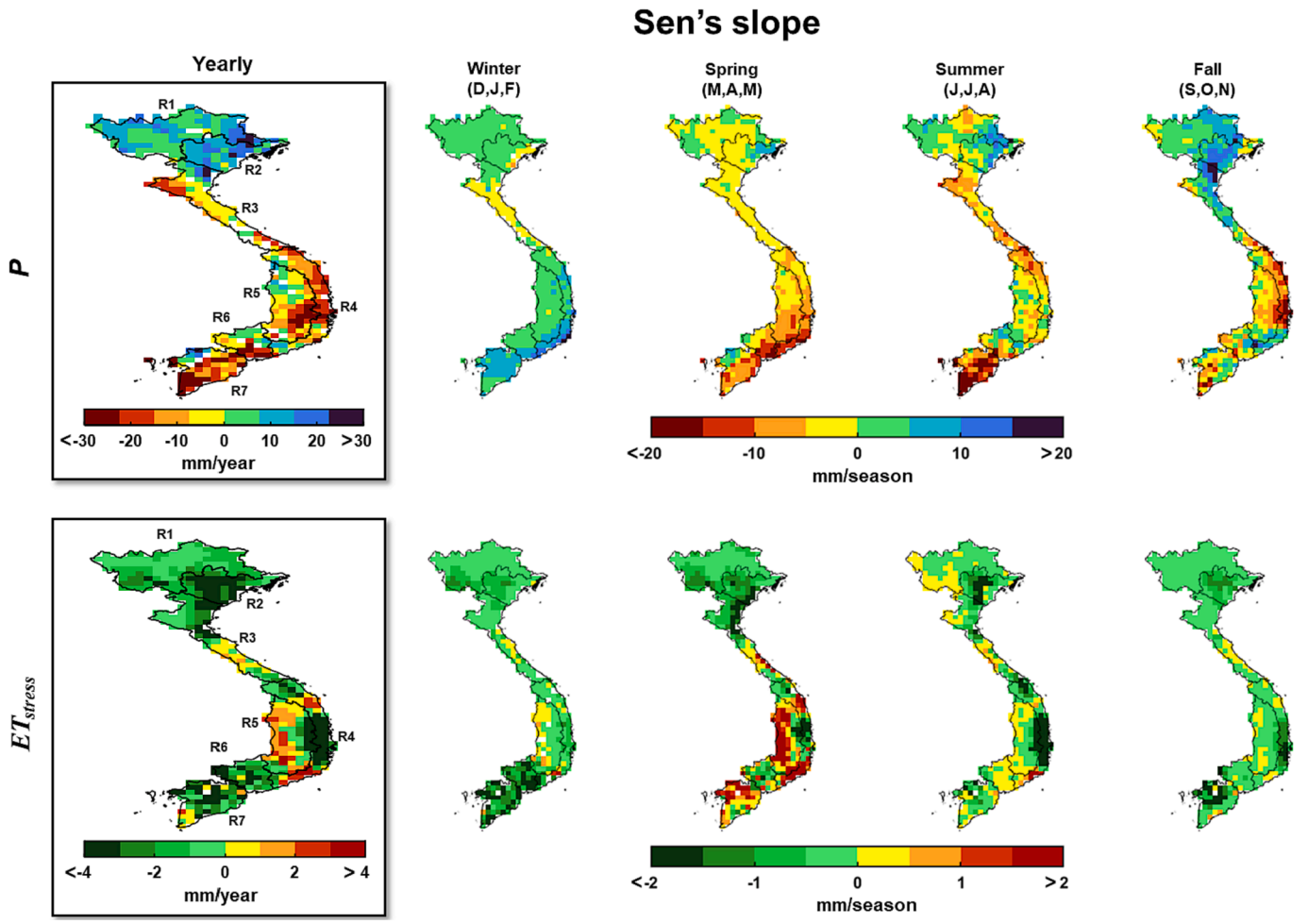

Fig. 4. Sen's slope of yearly and seasonal precipitation (P) and evaporative stress (ET_{stress} = PET-AET) during the study period in Vietnam.

warming effects on drought (Pei et al., 2018) but does not account for the actual moisture status of the soil and vegetation during extreme weather, which might be both reflected by AET and directly associated with agricultural drought (Vicente-Serrano et al., 2010). Furthermore, AET varies across different crops, and P has higher error than other variables (Kim and Rhee, 2016; Nguyen et al., 2023), so using SPEI to identify agricultural drought might retain some uncertainties. It is worth noting that this study does not refute the effectiveness of the SPEI in quantifying agricultural drought (as evidence of positive results showed in most regions, except R3-4). However, integrating the findings of this study with these in previously published reports lend us confidence that SESR, which incorporates AET in its calculations, is more suitable to capture agricultural drought condition under complex climate in several sub-regions of Vietnam. On the other hand, it is widely acknowledged that the SPEI is superior to other drought indexes in quantifying hydrological and ecological droughts in diverse of managed and natural systems (Beguería et al., 2014). Accordingly, R3 and R4 might suffer from longer drought durations in the form of transitions from hydrological and ecological droughts (reflected by the SPEI) to agricultural droughts (captured by the SESR) that potentially evolve during the rainy months. In agreement with Otkin et al. (2018), more than one type of drought can take place in a specific region in the same period, and possibly convert from one type of drought to another as its impacts and severities evolve. Generally, the SESR is able to capture the agricultural droughts in Vietnam and has the potential to detect agricultural flash drought events over the country. We suggest that future studies should apply multiple-indices to capture comprehensively characterizations of droughts over Vietnam.

5.3. Flash drought occurrence in Vietnam

Flash drought occurrence across Vietnam was detected using the SESR and incorporating multiple criteria related to rapid intensification and severity of drought as described in the methodology sections. Fig. 7 and Fig. 8 depict the spatial identification, characteristics, and drivers of flash drought over the study regions.

The results show that Vietnam has been suffering flash drought events, in which regions R1–3 only has a low f_D of flash drought, with an annual mean below 3 % per year and fewer than 9 events during the study period (Fig. 7a and Fig. 8a). Regions R4–7 mostly experienced a much higher f_D of flash drought, with an annual mean of up to 10 % per year and more than 9 events during the study period. The annual mean f_D of flash drought could exceed 12 % per year, with 15–21 events during study period in the central area of R5, the southeast of R4, and the majority of R6 and R7. A report by Christian et al. (2021) previously revealed that, in comparison with global hotpots (i.e., Brazil and India), the tropical Indochinese Peninsula of southeast Asia has experienced lesser but notable flash droughts. Regionally, the Lower Mekong River basin area in Cambodia and a portion of Vietnam (the central area of R5 and R7) regularly sees a higher frequency of flash drought events, compared with other areas in the basin (Kang et al., 2022). Additionally, ET_{stress} in the northern regions R1–3 is dramatically lower than in the southern regions R4–7 year-round due to different temperature and rainfall regimes, as discussed in Section 5.1.1, providing evidence for a higher f_D of flash drought in the southern R4–7 regions.

Otkin et al. (2018) underlined the need for multiple pathways of research to understand regional drivers and characteristics of flash

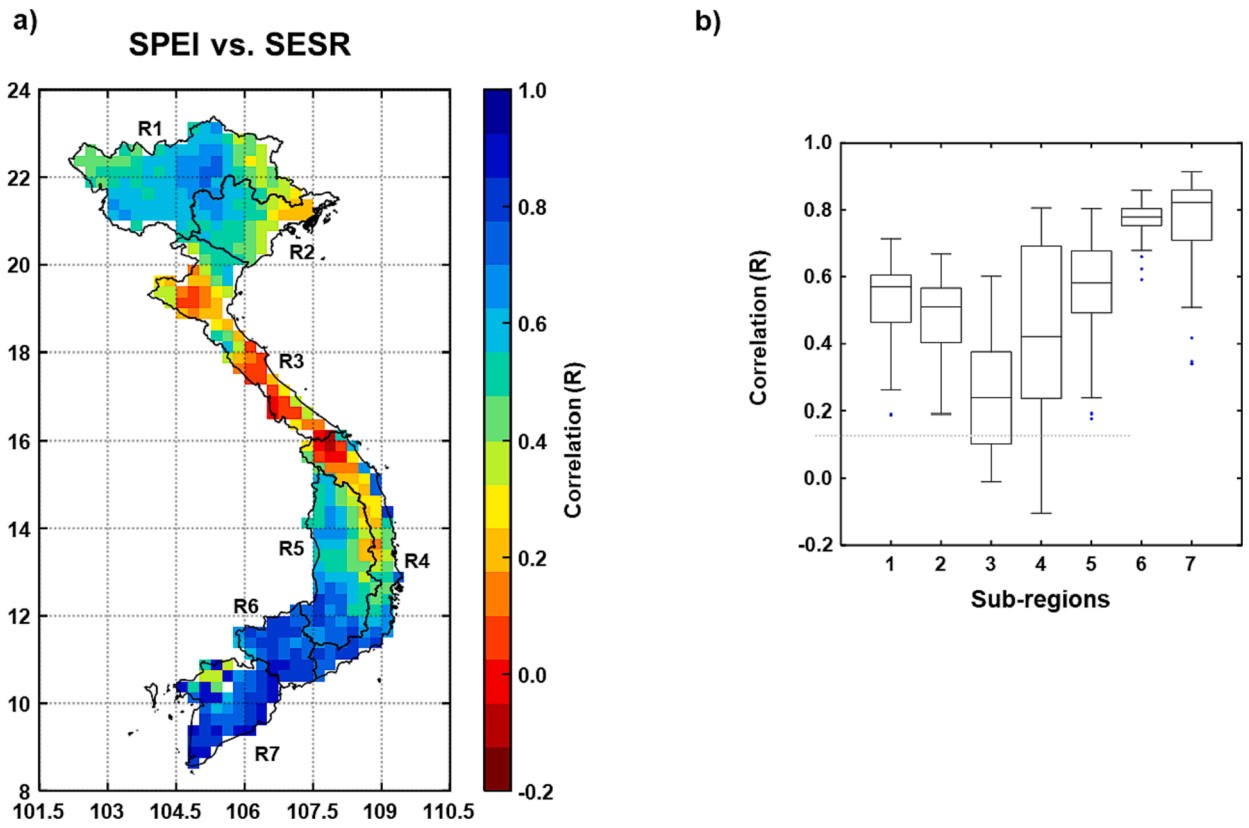

Fig. 5. Distribution of temporal correlations between SPEI and SESR over Vietnam (a) and boxplots for the seven sub-regions (b).

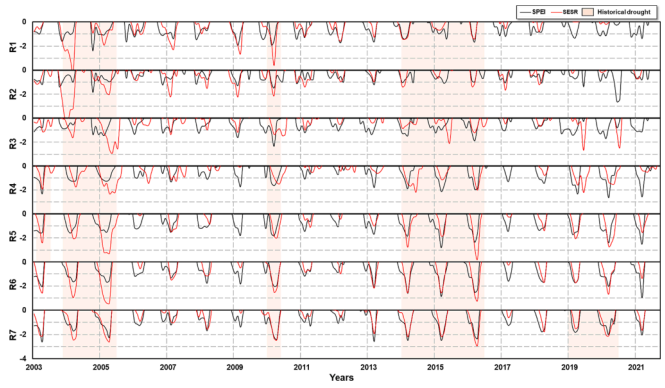

Fig. 6. Temporal variations in monthly SPEI and SESR for the seven sub-regions during the study period. Pink shades represent recorded historical droughts.

drought. Our study further found that flash droughts in the northern and southern regions of Vietnam exhibited distinguishable drought characteristics (Fig. 7b). Flash droughts tended to occur during the dry winter (December to February) in R1 and during hot summers (May to July) in R2 and R3 with small PDA magnitudes (below 20 % of each region's area. In the southern regions of R4–7, flash droughts frequently appeared during the dry season (December to April), and R7 in particular experienced a high f_D of flash droughts during the rainy season (July to August). Flash droughts predominantly occurred in less than 20 % of R4′s area, while it reached 30 % of regions R5–7, particularly region R5 and R6, where flash drought sometimes covered more than 50 % of the region. Most of sub-regions showed a decrease in PDA, most notably R5 and R6, which saw a statistically significant decline in PDA over the study period (Fig. 7b). From a climatological standpoint, changes in the occurrence and spatial extent of flash drought are a function of ET_{stress} according to variations in PET and AET. Specifically, an increase in PET can be associated with a rise in vapor pressure deficit and temperature, which are critical factors in climate change (Hobbins and Wood, 2012). One common feature over seven sub-regions is that of a high f_D of flash drought arising during times of high ET_{stress}, as discussed in Section 5.1.1. For example, in one year, R7 experienced a second period (July and August) with a relatively large f_D of flash drought, which can be attributed to the effects of a second intensification of ET_{stress} (Fig. 2). Likewise, the decline in PDA across most sub-regions was due to a decrease in ET_{stress} over the majority of Vietnam, as detailed in Section 5.1.2. It is worth clarifying that, despite the increase over time in ET_{stress} in regions R5 and R7, a reduction in PDA persisted over those areas. This can be mainly attributed to the fact that the ET_{stress} in these regions primarily escalated during the late dry season (March to May), whereas flash drought took place primarily during the early dry season (December to March), when such regions experienced reduced ET_{stress} (Fig. 3 and Fig. 4). Moreover, a change in the spatial coverage of a flash drought may be driven by a teleconnection phase (i.e., ENSO) (Christian et al., 2021). Consequently, decreases in PDA over most regions are possibly due to the weakness of El Niño events over the past two decades (Hu and Fedorov, 2018). The linkage between Vietnam flash droughts and ENSO climate modes is discussed in more detail in Section 5.4.

Next, to examine the drivers of flash droughts over the region of interest, standardized air temperature and PET anomalies at three ground stations in areas with large numbers of flash drought events were examined (Fig. 8b). The time series typically indicated that a flash drought event (light yellow) took place during periods when the SESR rapidly and significantly decreased (most often dropping below − 1) while anomalous air temperature and PET increased by more than 1 (Fig. 8b). This phenomenon was most evident during these selected flash drought events due to their rapid intensification over a relatively long period. Additionally, as noted in Section 5.1.1 and 5.1.2, ET_{stress}

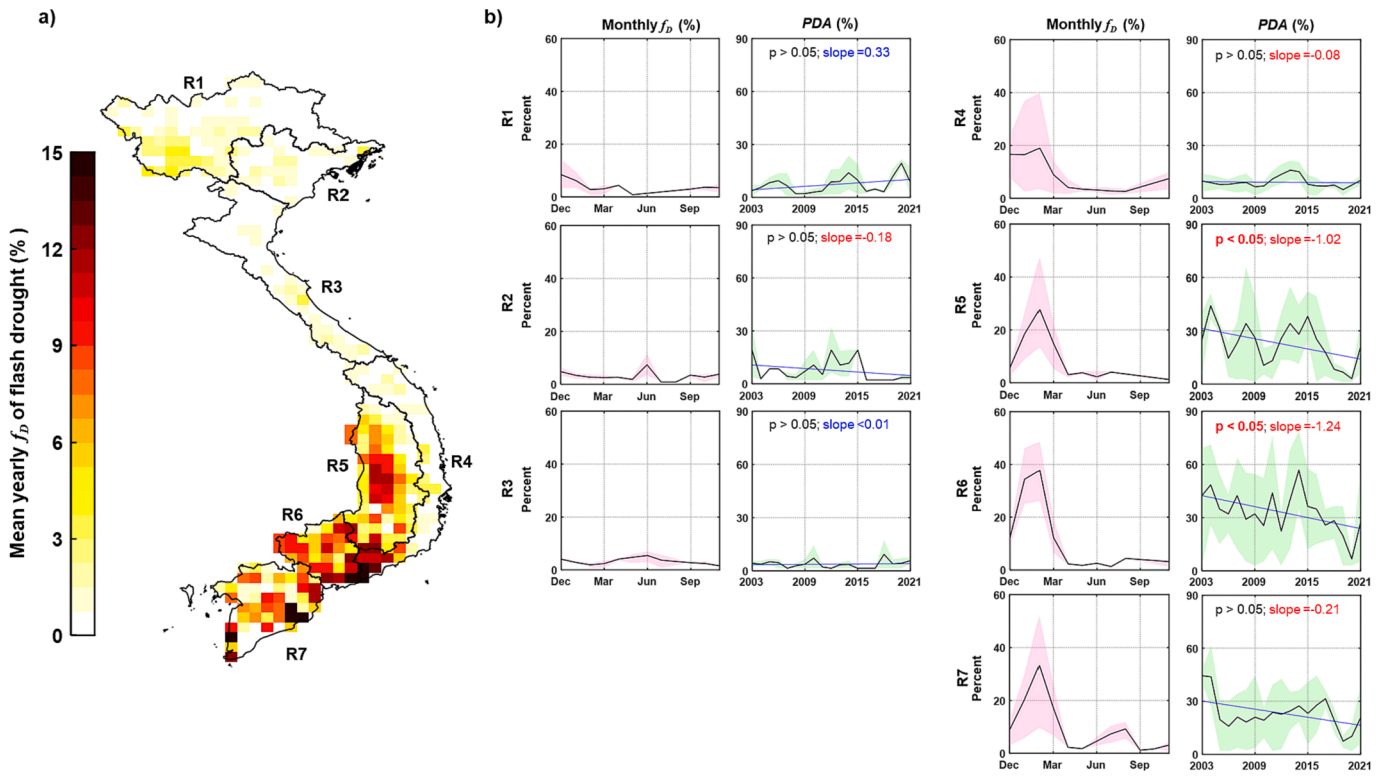

Fig. 7. Flash drought occurrence in Vietnam and its characteristics: (a) mean flash drought frequency is shown as the percentage of years during the study period (2003–2021); (b) monthly frequency of flash drought occurrence (f_D) and flash drought area percentage (PDA) in the seven sub-regions during the study period. Black lines, blue lines, and light pink and green shading denote the mean values, trend lines, and ranges from the second quantile to third quantiles values, respectively. 'Slope' in blue and red represents increasing and decreasing trends, respectively; and 'p-value' in red and bold indicates the statistical significance.

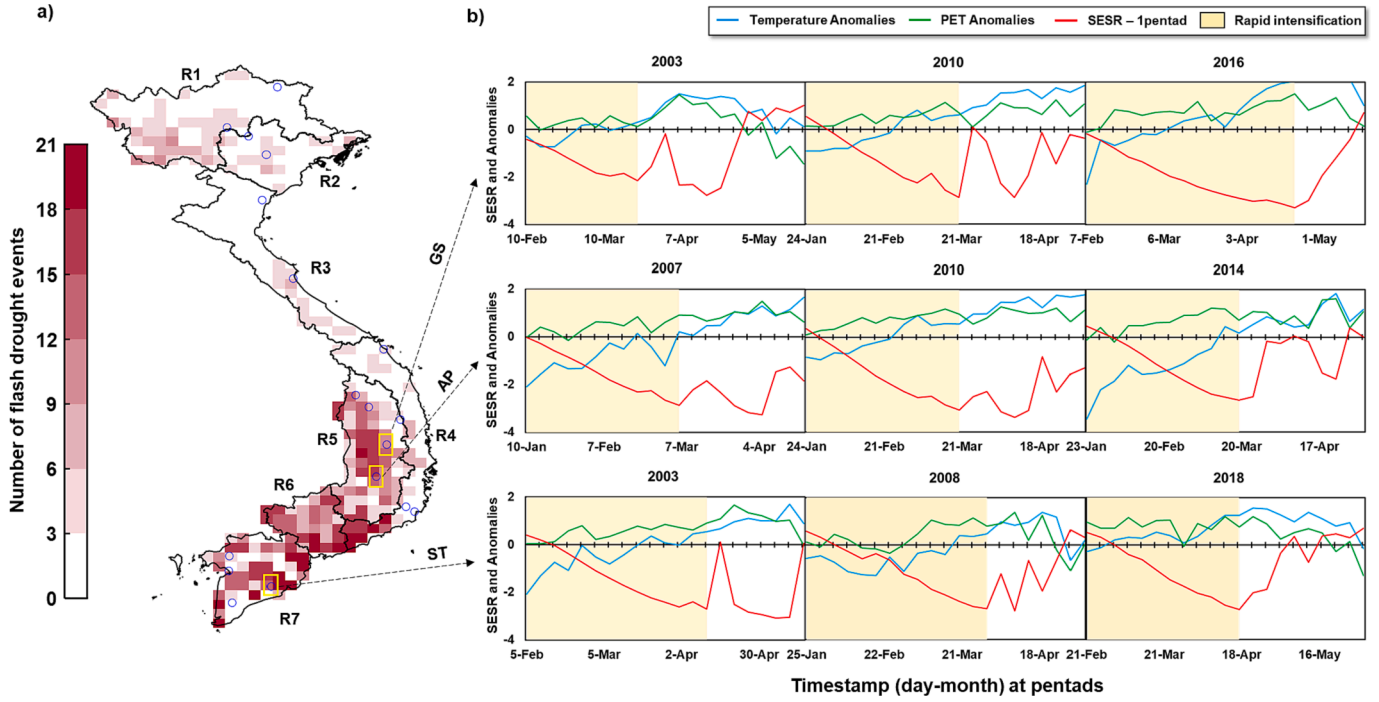

Fig. 8. Flash drought occurrence in Vietnam and its drivers. (a) Number of flash drought events occurring during the study period (2003–2021). (b) Examples of the evolution of flash drought events (SESR-1 pentad) along with standardized air temperature anomalies and standardized potential evapotranspiration anomalies at three stations in areas with a large number of flash drought occurrences.

conditions over Vietnam are insignificantly sensitive to P, and flash drought in the country can be categorized as 'heat wave' flash droughts due to their simultaneous manifestation during periods of elevated air temperatures and PET anomalies (Otkin et al., 2018). This type of flash drought can have profound impacts on vegetated areas (Otkin et al., 2018; Wang et al., 2016), suggesting an avenue for future research focusing on the impacts of flash drought on vegetation and crops in Vietnam. Overall, our study confirms that Vietnam has experienced flash drought events, particularly in the central highlands (R5), southeast (R6), and Mekong Delta River (R7), with approximately 12–21 events recorded over the last two decades, primarily in the dry season (December to April). Flash drought development in Vietnam is controlled by heat waves due to higher-than-normal air temperatures and PET. We therefore encourage more research on the interactions between heat wave flash droughts and agricultural impacts in Vietnam.

5.4. Impacts of ENSO on flash droughts in Vietnam

Identifying the teleconnection of ENSO with regional hydrology could bolster hydrological management efforts (Abtew and Trimble, 2010), we thus discuss the linkage between flash drought and ENSO phase in this section. Initially, the correlation between the monthly mean SESR and monthly ENSO indices is represented by a spatial distribution of R values in Vietnam (Fig. 9). Signs of ONI, Niño 3.4, and MEI were inverted to consistently indicate El Niño and La Niña events in the same manner as other indices, such that negative values of ENSO indices now represent El Niño and vice versa. This section also investigates patterns of yearly frequencies of flash droughts in the southern R4–7 regions, which have the highest f_D rates in the country, along with ENSO events, as shown by the ONI over study periods as the time series illustrates in Fig. 10.

Throughout the country, spatial maps indicate discrepancies in relationships between the SESR and ENSO indices among sub-regions (Fig. 9). In northern regions, the association between the SESR and the five ENSO indices is generally weak (with most R values below 0.2) in R1, R3 and the northern portion of R4, whereas R2 exhibited a slightly higher association (R values within a range of 0.2–0.3) with ONI, Niño 3.4, and MEI indices. Unlike the northern regions, the SESR showed a markedly stronger correlation (R varies within a range of 0.3–0.6), with all five ENSO indices for the southern regions (R5–7 and the southeast area of R4), and a particularly large correlation evident between the SESR and TNI (most R values above 0.5). More precisely, time series analysis of ENSO events and flash drought occurrence in R4-7 further revealed a similar pattern of flash drought occurrence and ENSO climate mode (Fig. 10). Years characterized by La Niña events (2006, 2008–2009, 2011–2012, and 2017–2018) were associated with a low f_D of flash drought (mostly below or around 10 % per year), whereas those featuring El Niño events (2003, 2005, 2007, 2010, 2016–2017, and 2019) were involved in a significantly higher f_D of flash drought, ranging from 12 % to 20 % per year. Surprisingly, years with neutral conditions (2004, 2013–2014, and 2020) showed a considerable f_D of flash drought of approximately 15 % per year, particularly in 2004, when the flash drought occurrence rate in R6 approached nearly 30 %. Generally, flash droughts in Vietnam are influenced by the ENSO climate mode, with a significant correlation identified in southern regions (R4–7) and a less pronounced connection in the north (R1–3).

Historically, during years with El Niño events, prolonged drought events would commonly occur over all of Vietnam (Le et al., 2020, 2019). Statistically, Christian et al. (2021) found that the Indochinese Peninsula was one of a few regions in the world (along with southwest Africa and northwest North America) to show a significant association between flash drought events and ENSO climate modes. It is therefore not surprising that the ENSO phase also had impacts on flash drought events in Vietnam. Among sub-regions, the contrasting association between ENSO events and flash droughts in the northern and southern regions was likely the result of the diverse rainfall regimes and temperature conditions over these areas. While rainfall and temperature in Northern R1-3 are mainly dominated by the East Asian summer monsoon system (Buckly et al., 2014), those in the southern R4–7 regions are driven by the southeast Asian summer monsoon climate (Yan et al., 2018). Compared with the East Asian monsoon, the Southeast Asian summer monsoon is closer to the equator, where the warmest sea-surface temperature has been reported, along with the strongest example of coupling between ocean and atmospheric circulation. Moreover, peak ENSO events regularly take place from October to March, coinciding with a cool fall and cold winter in northern regions (Section 5.1.1), when flash droughts occur infrequently (Section 5.3). Any direct link between ENSO and flash drought in these regions is unclear but cannot be ruled out, as evidence of a correlation between the SESR and ENSO indices was found in this study. In contrast, peak ENSO times coincided with the dry season of southern regions in Vietnam (December to April) (Section 5.1.1), when flash droughts occur most frequently in such regions (Hu and Fedorov, 2018), suggesting a stronger susceptibility of flash droughts to ENSO effects in the south than in

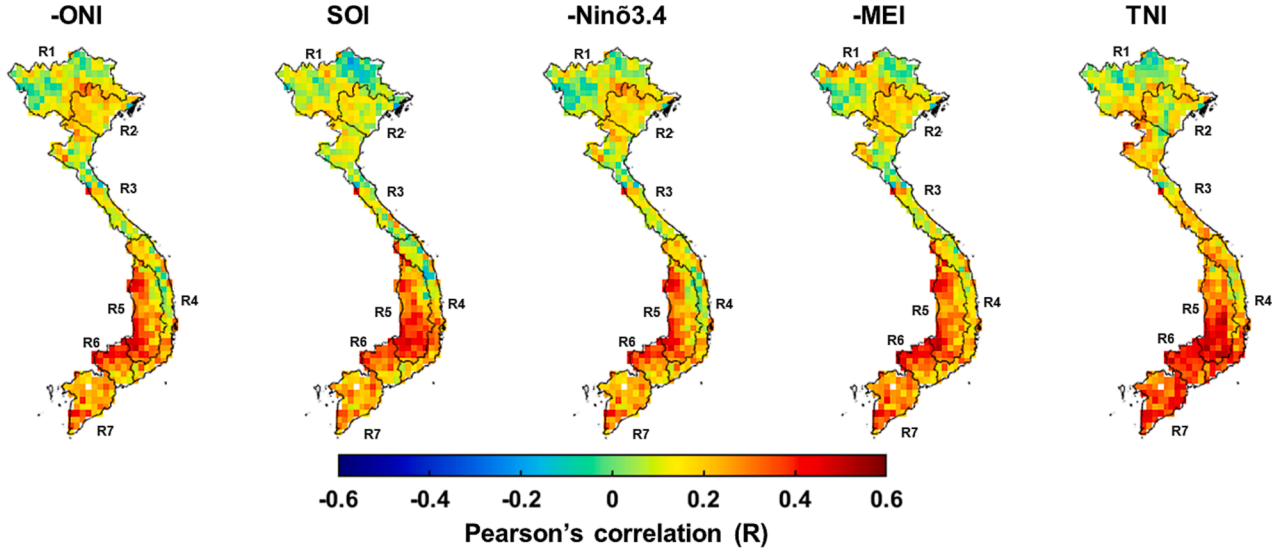

Fig. 9. Pearson's correlations between the negative SESR and five climate variables at the monthly scale across the study region. The signs of the ONI, Niño3.4, and MEI are reversed to indicate El Niño and La Niña events in the same manner as the other indices.

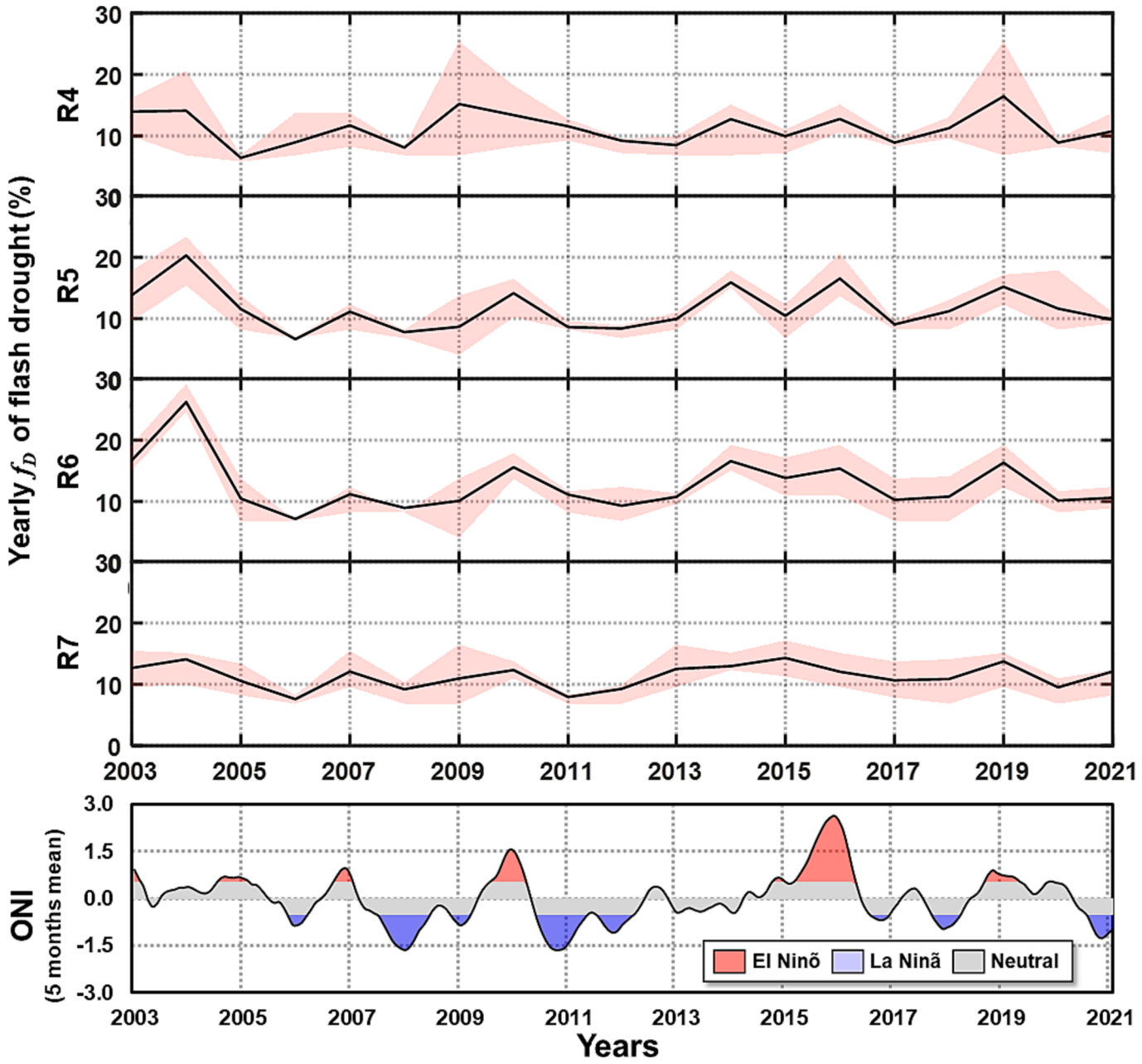

Fig. 10. Temporal variation between the yearly frequency of flash droughts in the four sub-regions (R4-7) with the highest occurrence rates and the Oceanic Nino Index.

the north of Vietnam.

Delving deeper into the influences of ENSO on flash drought in Southern Vietnam, this study found that the frequency of flash drought occurrence rose in El Niño years while low frequencies were associated with La Niña years. The El Niño phase typically reinforces the hotter- and drier-than-normal conditions over southeast Asia (Juneng and Tangang, 2005), as evaporative demand in the atmosphere rises, resulting in drought events. Under such a weather context, the rapid intensification of evaporative stress could lead to the onset of flash drought. Conversely, La Niña years are accompanied by wetter- and cooler-than-normal conditions that reduce the likelihood of flash droughts (Christian et al., 2021). By those definitions, neutral years inherently have a greater possibility of complex dry and hot events than do La Niña years, particularly during neutral years that is followed by an El Niño year with much hotter and drier conditions (Feng and Hao, 2021). For example, 2004 was an ENSO-neutral year sandwiched between two El Niño years (2003 and 2005), which apparently experienced a prolonged dry and hot extreme, followed by a high frequency of flash drought occurrence. Overall, flash drought occurrence in Vietnam is closely related to ENSO events, with a notable emphasis in southern regions, where flash drought can be promoted during either El Niño or neutral conditions.

6. Conclusions

This paper aimed to investigate the occurrence and characteristics of flash droughts in Vietnam, along with its driving factors such as rainfall, evaporative stress, and ENSO phases. It focused on: (1) tracking flash drought occurrence and its characteristics in Vietnam using the SESR and flash drought criteria, and (2) examining the impacts of ENSO phase on flash drought occurrence in Vietnam.

In term of quantifying drought conditions, monthly SESR values

effectively presented historical drought events over the study period and closely matched the SPEI over most study regions, with the exception of the Central Coast (R3 and R4). As Vietnam potentially undergoes more than one drought type on the same periods, using a single drought index therefore cannot adequately reflect the features and duration of drought in Vietnam, particularly in areas with complicated climate conditions (i.e., the central coastal region, R3 and R4).

By incorporating four strict criteria that fully describe the characteristics of a flash drought event into pentad SESR calculations and their ΔSESR, this study successfully detected flash drought occurrence over Vietnam. Over the last two decades, regions R1–3 and the majority of R4 endured fewer than 9 flash drought events, most covering less than 20 % of drought area, while the remaining areas (R5–7 and the southeast area of R4) underwent between 12 and 21 events covering from 30 % to over 50 % of each region's area. Characteristically, flash drought events primarily occurred during dry winters in the northern R1 region, during hot summers in northern regions R2 and R3, and during the dry season in southern regions R4–7, most notably when anomalous PET and temperatures were positive and exacerbating. We also found that the ENSO climate mode affected flash drought occurrence in Vietnam, with a notable association in the southern R5–7 regions, where a high flash drought frequency can appear in either El Niño or neutral conditions. During La Niña years, the occurrence of flash drought is less likely but still possible, highlighting the need for ongoing preparedness and readily available impact mitigation strategies. Overall, our study once again confirmed the occurrence of flash drought extreme events over Vietnam, particularly in southern regions of the country. These bridges a research gap in our understanding of the characteristics and drivers of drought occurrences in Vietnam, which gives an idea of where our findings fall among existing Vietnam drought publications. We encourage more research to better understand the impacts of flash droughts on agriculture and other aspects of Vietnam as well as other agriculture-oriented countries.

CRediT authorship contribution statement

Ngoc My Nguyen: Conceptualization, Methodology, Resources, Software, Formal analysis, Writing – original draft, Visualization. **Minha Choi:** Supervision, Project administration, Funding acquisition, Writing – review & editing.

Declaration of competing interest

The authors declare that they have no known competing financial interests or personal relationships that could have appeared to influence the work reported in this paper.

Data availability

The authors do not have permission to share data.

Acknowledgments

This research was supported by a grant (2021-MOIS35-003) of 'Policy-linked Technology Development Program on Natural Disaster Prevention and Mitigation' funded by Ministry of Interior and Safety (MOIS, Korea). This research was supported by the BK21 FOUR (Fostering Outstanding Universities for Research) funded by the Ministry of Education (MOE, Korea) and National Research Foundation of Korea (NRF). The authors are grateful to the developers, managers, and funding organizations for freely providing GLEAM evapotranspiration data, IMERG rainfall products, and ENSO climate indices.

References

Abtew, W., Trimble, P., 2010. El Niño-southern oscillation link to south florida hydrology and water management applications. Water Resour. Manag. 24, 4255–4271. https://doi.org/10.1007/s11269-010-9656-2.

Aghakouchak, A., Cheng, L., Mazdiyasni, O., A.f.,, 2014. Global warming and changes in risk of concurrent climate extremes: Insights from the 2014 California drought. Geophys. Res. Lett. https://doi.org/10.1002/2014GL062308.

Beck, H.E., Zimmermann, N.E., McVicar, T.R., Vergopolan, N., Berg, A., Wood, E.F., 2018. Present and future Koppen-Geiger climate classification maps at 1-km resoluation. Scientific Data 5, 180214. https://doi.org/10.1038/s41597-020-00616-w.

Beguería, S., Vicente-Serrano, S.M., Reig, F., Latorre, B., 2014. Standardized precipitation evapotranspiration index (SPEI) revisited: parameter fitting, evapotranspiration models, tools, datasets and drought monitoring. Int. J. Climatol. 34, 3001–3023. https://doi.org/10.1002/joc.3887.

Buckly, B.M., Fletcher, R., Wang, S.S., Zottoli, B., Pottier, C., 2014. Monsoon extremes and society over the past millennium on mainland Southeast Asia. Quat. Sci. Rev. J. 1–19 https://doi.org/10.1016/j.quascirev.2014.04.022.

Christian, J.I., Basara, J.B., Otkin, J.A., Hunt, E.D., Wakefield, R.A., Flanagan, P.X., Xiao, X., 2019. A methodology for flash drought identification: Application of flash drought frequency across the United States. J. Hydrometeorol. 20, 833–846. https://doi.org/10.1175/JHM-D-18-0198.1.

Christian, J.I., Basara, J.B., Hunt, E.D., Otkin, J.A., Mishra, V., Xiao, X., Randall, R.M., Furtado, J.C., 2021. Global distribution, trends, and drivers of flash drought occurrence. Nat. Comnunications 1–11. https://doi.org/10.1038/s41467-021-26692-z.

Dai, A., 2012. Increasing drought under global warming in observations and models. Nat. Clim. Chang. 1–15 https://doi.org/10.1038/NCLIMATE1633.

Donohue, R.J., McVicar, T.R., Roderick, M.L., 2010. Assessing the ability of potential evaporation formulations to capture the dynamics in evaporative demand within a changing climate. J. Hydrol. 386, 186–197. https://doi.org/10.1016/j.jhydrol.2010.03.020.

Feng, S., Hao, Z., 2021. Quantitative contribution of ENSO to precipitation-temperature dependence and associated compound dry and hot events. Atmos. Res. 260, 105695 https://doi.org/10.1016/j.atmosres.2021.105695.

Forda, T.W., Labosier, C.F., 2017. Meteorological conditions associated with the onset of flash drought in the Eastern United States. Agric. for. Meteorol. 414–423. https://doi.org/10.1016/j.agrformet.2017.08.031.

Gocic, M., Trajkovic, S., 2013. Analysis of changes in meteorological variables using Mann-Kendall and Sen's slope estimator statistical tests in Serbia. Glob. Planet. Change 100, 172–182. https://doi.org/10.1016/j.gloplacha.2012.10.014.

Godfray, H.C.J., Beddington, J.R., Crute, I.R., Haddad, L., Lawrence, D., Muir, J.F., Pretty, J., Robinson, S., Thomas, S.M., Toulmin, C., 2010. Food security: the challenge of feeding 9 billion people. Science 327, 812–818. Science (80-).

Hamed, K.H., 2009. Exact distribution of the Mann-Kendall trend test statistic for persistent data. J. Hydrol. https://doi.org/10.1016/j.jhydrol.2008.11.024.

Hamed, K.H., Rao, A.R., 1998. A modified Mann-Kendall trend test for autocorrelated data. J. Hydrol. 204, 182–196. https://doi.org/10.1016/j.atmosres.2018.06.019.

Hobbins, M., Wood, A., 2012. What drives the variability of evaporative demand across the conterminous united states? J. Hydrometeorol. https://doi.org/10.1016/10.1175/JHM-D-11-0101.1.

Hobbins, M.T., Wood, A., McEvoy, D.J., Huntington, J.L., Morton, C., Anderson, M., Hain, C., 2016. The evaporative demand drought index. Part I: Linking drought evolution to variations in evaporative demand. J. Hydrometeorol. 17, 1745–1761. https://doi.org/10.1175/JHM-D-15-0121.1.

Hu, S., Fedorov, A.V., 2018. Cross-equatorial winds control El Niño diversity and change. Nat. Clim. Chang. 8, 798–802. https://doi.org/10.1038/s41558-018-0248-0.

Hu, X., Ren, H., Tansey, K., Zheng, Y., Ghent, D., Liu, X., Yan, L., 2019. Agricultural drought monitoring using European Space Agency Sentinel 3A land surface temperature and normalized difference vegetation index imageries. Agric. for. Meteorol. 279, 107707 https://doi.org/10.1016/j.agrformet.2019.107707.

Huffman, G.J., Bolvin, D.T., Nelkin, E.J., Tan, J., 2020. Integrated Multi-satellitE Retrievals for GPM (IMERG) Technical Documentation. Am. J. Orthodontics Dentofacial Orthopedics. https://doi.org/10.1016/j.ajodo.2020.07.011.

Huffman, G.J., 2018. NASA Global Precipitation Measurement (GPM) Integrated Multi-satellitE Retrievals for GPM (IMERG).

Juneng, L., Tangang, F.T., 2005. Evolution of ENSO-related rainfall anomalies in Southeast Asia region and its relationship with atmosphere - Ocean variations in Indo-Pacific sector. Clim. Dyn. https://doi.org/10.1007/s00382-005-0031-6.

Kang, H., Sridhar, V., Ali, S.A., 2022. Climate change impacts on conventional and flash droughts in the Mekong River Basin. Sci. Total Environ. 838, 155845 https://doi.org/10.1016/j.scitotenv.2022.155845.

Kiladis, G.N., van Loon, H., 1988. The Southern Oscillation. Part VII: Meteorological anomalies over the Indian and Pacific sectors associated with the extremes of the oscillation. Mon. Wea. Rev. 116, 120–136.

Kim, D., Rhee, J., 2016. A drought index based on actual evapotranspiration from the Bouchet hypothesis. Geophys. Res. Lett. 43, 10277–10285. https://doi.org/10.1002/2016GL070302.

Le, M.H., Kim, H., Moon, H., Zhang, R., Lakshmi, V., Nguyen, L.B., 2020. Assessment of drought conditions over Vietnam using standardized precipitation evapotranspiration index, MERRA-2 re-analysis, and dynamic land cover. J. Hydrol. Reg. Stud. 32, 100767 https://doi.org/10.1016/j.ejrh.2020.100767.

Le, P.V.V., Phan-Van, T., Mai, K.V., Tran, D.Q., 2019. Space–time variability of drought over Vietnam. Int. J. Climatol. 39, 5437–5451. https://doi.org/10.1002/joc.6164.

Li, J., Wang, Z., Wu, X., Chen, J., Guo, S., Zhang, Z., 2020. A new framework for tracking flash drought events in space and time. Catena 194, 104763. https://doi.org/10.1016/j.catena.2020.104763.

Lyon, B., 2004. The strength of El Niño and the spatial extent of tropical drought Bradfield. Geophys. Res. Lett. 31, L21204. https://doi.org/10.1029/2004GL020901.

Miralles, D.G., Holmes, T.R.H., De Jeu, R.A.M., Gash, J.H., Meesters, A.G.C.A., Dolman, A.J., 2011. Global land-surface evaporation estimated from satellite-based observations. Hydrol. Earth Syst. Sci. 15, 453–469. https://doi.org/10.5194/hess-15-453-2011.

Miralles, D.G., Jiménez, C., Jung, M., Michel, D., Ershadi, A., Mccabe, M.F., Hirschi, M., Martens, B., Dolman, A.J., Fisher, J.B., Mu, Q., Seneviratne, S.I., Wood, E.F., Fernández-Prieto, D., 2016. The WACMOS-ET project - Part 2: Evaluation of global terrestrial evaporation data sets. Hydrol. Earth Syst. Sci. https://doi.org/10.5194/hess-20-823-2016.

Narasimhan, B., Srinivasan, R., 2005. Development and evaluation of Soil Moisture Deficit Index (SMDI) and Evapotranspiration Deficit Index (ETDI) for agricultural drought monitoring. Agric. for. Meteorol. 133, 69–88. https://doi.org/10.1016/j.agrformet.2005.07.012.

Nguyen, M.N., Choi, M., 2022. Advances in evapotranspiration prediction using gross primary productivity based on eco-physiological constraints. Hydrol. Process. 36, 1–19. https://doi.org/10.1002/hyp.14628.

Nguyen, N.M., Choi, M., 2023. Evapotranspiration partitioning and agricultural drought quantification with an optical trapezoidal framework. Agric. for. Meteorol. 338, 109520 https://doi.org/10.1016/j.agrformet.2023.109520.

Nguyen, D.Q., Renwicks, J., McGregor, J., 2014. Variations of surface temperature and rainfall in Vietnam from 1971 to 2010. R. Meteorol. Soc. 34, 249–264. https://doi.org/10.1002/joc.3684.

Nguyen, H., Shaw, R., 2011. Drought risk management in Vietnam. Chapter 8 Droughts in Asian Monsoon Region. Emerald Group Publishing Limited, Bingley, UK, pp. 141–161.

Otkin, J.A., Anderson, M.C., Hain, C., Mladenova, I.E., Basara, J.B., Svoboda, M., 2013. Examining rapid onset drought development using the thermal infrared-based evaporative stress index. J. Hydrometeorol. 14, 1057–1074. https://doi.org/10.1175/JHM-D-12-0144.1.

Otkin, J.A., Shafer, M., Svoboda, M., Wardlow, B., Anderson, C., Hain, C., Basara, J., 2015. Facilitating the Use of Drought Early warning information through intertations with Agricultural Stakeholders. Am. Meteorol. Soc. https://doi.org/10.1175/BAMS-D-14-00219.1.

Otkin, J.A., Svoboda, M., Hunt, E.D., Ford, T.W., Anderson, M.C., Hain, C., Basara, J.B., 2018. Flash droughts: A review and assessment of the challenges imposed by rapid-onset droughts in the United States. Bull. Am. Meteorol. Soc. 99, 911–919. https://doi.org/10.1175/BAMS-D-17-0149.1.

Paul, G., Agrawal, N., Dollar, D., 2004. Economic Growth, Poverty, and Household Welfare in Vietnam. World Bank regional and sectoral studies. ISBN 0-8213-5543-0.

Pei, W., Fu, Q., Liu, D., Li, T., 2018. A drought index for Rainfed agriculture: The Standardized Precipitation Crop Evapotranspiration Index (SPCEI). Hydrol. Process. 33, 803–815. https://doi.org/10.1002/hyp.13365.

Sen, P.K., 1968. Estimates of the Regression Coefficient Based on Kendall's Tau. J. Am. Stat. Assoc. 324, 1379–1389. http://www.jstor.org/stable/2285891.

Smith, A.B., Katz, R.W., 2013. US billion-dollar weather and climate disasters: Data Sources, Trends. Accuracy and Biases. Nat. Hazards 67, 387–410. https://doi.org/10.1007/s11069-013-0566-5.

Stojanovic, M., Liberato, M.L.R., Sorí, R., Vázquez, M., Tan, P.V., Hieu, D.V., Cong, T.H., Nguyen, P.N.B., Nieto, R., Gimeno, L., 2020. Trends and Extremes of Drought Episodes in Vietnam Sub-Regions during 1980–2017 at Different Timescales. Water (switzerland) 12, 813. https://doi.org/10.3390/w12030813.

Thanh, H.V., Duc, T.N., Van, T.P., 2014. Evolution of meteorological drought characteristics in Vietnam during the 1961–2007 period. Theory Appl. Climatol. 118, 367-375. https://doi.org/ 10.1007/s00704-013-1073-z.

Trenberth, K.E., Stepaniak, D.P., 2001. Indices of El Nino Evolution. J. Climate 14, 1697–1701.

Tue, V.M., Raghavan, S.V., Minh, P.D., Shie-Yui, L., 2015. Investigating drought over the Central Highland, Vietnam, using regional climate models. J. Hydrol. 526, 265–273. https://doi.org/10.1016/j.jhydrol.2014.11.006.

Ty, T.V., Lavane, K., Nguyen, P.C., Downes, N.K., Nam, N.D.G., Minh, H.V.T., Kumar, P., 2022. Assessment of Relationship between Climate Change, Drought, and Land Use and Land Cover Changes in a Semi-Mountainous Area of the Vietnamese Mekong Delta. Land. https://doi.org/10.3390/land11122175.

Vicente-Serrano, S.M., 2010. A New Global 0.58 Gridded Dataset (1901–2006) of a Multiscalar Drought Index: Comparison with Current Drought Index Datasets Based on the Palmer Drought Severity Index S. J. Hydrometeorol. https://doi.org/10.1175/2010JHM1224.1.

Wang, L., Yuan, X., Xie, Z., Wu, P., Li, Y., 2016. Increasing flash droughts over China during the recent global warming hiatus. Sci. Rep. 6, 1–8. https://doi.org/10.1038/srep30571.

Wolter, K., Timlin, M.S., 1993. Monitoring ENSO in COADS with a seasonally adjusted principal component index. Proc. of the 17th Climate Diagnostics Workshop. CIMMS and the School of Meteor., Univ. of Oklahoma, Norman, OK, NOAA/NMC/CAC, NSSL, Oklahoma Clim. Survey, pp. 52–57.

Wolter, K., Timlin, M.S., 1998. Measuring the strength of ENSO events - how does 1997/98 rank? Weather 53, 315–324. https://doi.org/10.1002/j.1477-8696.1998.tb06408.x.

Yan, X., Konopka, P., Ploeger, F., Tao, M., Muller, R., Michelle, L.S., Bian, J., Riese, M., 2018. El Niño Southern Oscillation influence on the Asian summer monsoon anticyclone. Atmos. Chem. Physic 18, 8079–8096.

Yao, N., Li, Y., Lei, T., Peng, L., 2018. Drought evolution, severity and trends in mainland China over 1961–2013. Sci. Total Environ. 616–617, 73–89. https://doi.org/10.1016/j.scitotenv.2017.10.327.

Yao, Y., Liang, S., Qin, Q., Wang, K., 2010. Monitoring drought over the conterminous United States using MODIS and NCEP reanalysis-2 data. J. Appl. Meteorol. Climatol. 49, 1665–1680. https://doi.org/10.1175/2010JAMC2328.1.

Zaki, M.K., Noda, K., 2022. A Systematic Review of Drought Indices in Tropical Southeast Asia. Atmosphere (basel). https://doi.org/10.3390/atmos13050833.

J. Zhou Y. Wang B. Su A. Wang H. Tao J. Zhai Z.W. Kundzewicz T. Jiang, 2020.Choice of potential evapotranspiration formulas influences drought assessment: A case study in China. 242, 104979. https://doi.org/10.1016/j.atmosres.2020.104979.